Received: March 2, 2020. Revised: April 21, 2020.

INASS

International Journal of
Intelligent Engineering & Systems

http://www.inass.org/

Optimal Antenna Slot Design for Hepatocellular Carcinoma Microwave Ablation Using Multi-Objective Fuzzy Decision Making

Petch Nantivatana[1]* Pattarapong Phasukkit[2] Supan Tungjitkusolmun[3]
Keerati Chayakulkheeree[4]

[1]*Faculty of Digital Technology, Chitralada Technology Institute, Thailand*
[2]*Department of Electronics Engineering, Faculty of Engineering,*
King Mongkut's Institute of Technology Ladkrabang, Thailand
[3]*Department of Biomedical Engineering, Faculty of Engineering,*
King Mongkut's Institute of Technology Ladkrabang and CMKL University, Thailand
[4]*School of Electrical Engineering, Institute of Engineering, Suranaree University of Technology, Thailand*
* Corresponding author's Email: petch.nan@cdti.ac.th, petch.nant@gmail.com

Abstract: This paper presents the optimal antenna slot position and sizing (OASPS), for microwave (MW) hepatocellular carcinoma (HCC) treatment, using multi-objective fuzzy decision making (MOFDM). In the optimal design problem formulation, the multi-objective for, (1) achievement for a near-spherical zone for ablation defined by axial ratio (*AR*), (2) the minimum reflection coefficient (S_{11}), and (3) maximum volume of destroying (*VD*), are desired. The finite element method (FEM) is used for MW distribution simulation for coordination analysis with the proposed MOFDM based OASPS. The investigation on the design results shown that the temperature distribution of the proposed MOFDM for OASPS is in the more controllable shape comparing to the existing design, due to the sharp beam of temperature distribution to the target at the front side of slot with the less temperature distribution at the rare side of slot. The results also show that the proposed MOFDM for OASPS for OASPS design is easier to manage with the less effect to the rare side of the slot. Moreover, the proposed MOFDM for OASPS resulted in the temperature distribution shape closer to round shape than the existing design. The MOFDM for OASPS is tested on designing of the antenna build up from the coaxial cable. The coaxial cable used is Semi-rigid 141 (RG402 M17/130-RG402 Copper Jacket) including Inner conductor, Dielectric, and Outer conductor. In the simulation, the slot distance from conductor end (L_{ts}), representing the slot position, is varied as 2.3mm, 3.3mm, 4.3mm, 5.3mm, 6.3mm, 7.3mm, and 8.3mm. Meanwhile, the slot size (W_d), is varied as 1mm, 2mm, 3mm, 4mm, 5mm, and 6mm. The input power (P_i) used is 50 W with the duration of 300 seconds. The comparison of obtained by different L_{ts} and W_d, is investigated. The simulation results show that the proposed MOFDM based OASPS can efficiently and effectively provide the near-spherical zone of ablation result with simultaneously trade-off between S_{11} minimization and *VD* maximization.

Keywords: Microwave ablation, Hepatocellular carcinoma treatment, Finite element method, Multi-objective fuzzy decision making.

Abbreviations

BCLC	Barcelona Clinic Liver Cancer
FEM	finite element method
HCC	hepatocellular carcinoma
HIFU	high intensive focused ultrasound
MCT	microwave coagulation therapy
MOFDM	multi-objective fuzzy decision making
MW	microwave
MWA	microwave ablation
OASPS	optimal antenna slot position and sizing
RFA	radiofrequency ablation

Symbols

S_{11}	reflection coefficient (*dB*)
SAR	specific absorption rate (W/kg)
VD	volume of destroying (mm^3)
AR	axial ratio
ARC	circular condition of axial ratio
C	the specific heat of tissue (J/kg.K)
k	thermal conductivity of tissue (W/m.K)

Received: March 2, 2020. Revised: April 21, 2020.

T tissue temperature (°C)
Q_p the heat loss due to microvascular blood perfusion (W/m^3)
Q_m the energy from metabolic processes (W/m^3)
Q_{ext} the external heat source (W/m^3)
ρ the density of tissue (kg/m^3)
σ the conductivity of tissue (S/m)
E the electric field intensity (V/m)
P_r the reflected power (W) and
P_i the input power (W)

1. Introduction

In recent day, the primary liver cancer, especially hepatocellular carcinoma (HCC), remains a considerable disease in the world. It is one of the three highest causes of cancer death in the Asia Pacific region [1]. In Thailand, HCC is ubiquitous with the incidence rate of approximately 180 per 100,000 persons at the age between 60–65. However, HCC surveillance programs are still not commonly available in Thailand, especially in the rural area.

Barcelona Clinic Liver Cancer (BCLC) classified the HCC treatment into two groups [2, 3], which are, (1) treatment with curative intention (resection surgery, liver transplantation, local ablation via percutaneous ethanol injection or radiofrequency ablation, and palliative treatments, such as transarterial chemoembolization, new molecular target therapies) and (2) symptomatic treatment. The outcome prediction and treatment allocation of HCC patients can be categorized into 5 stages (0, A, B, C and D), as shown in Fig. 1 [2, 3]. The best outcomes have been reported in Child–Pugh A patients with small single tumors, which are commonly less than 2cm in diameter and Child–Pugh B treatment of patients with the larger tumors of 3–5cm and multiple tumors (3 nodules <3cm) with non-surgical small tumors. Meanwhile, microwave ablation (MWA), laser ablation and cryo-ablation have been proposed for local ablation in HCC.

Ordinarily, local ablation is the first option recommended for remedying at the earlier stages HCC. The treatment includes, thermal ablative therapies emerged including hyperthermic treatments (heating of tissue at 50–100°C) using radiofrequency ablation (RFA), MWA, high intensive focused ultrasound (HIFU) [4] and laser ablation, and tissue freezing therapy by cryo-ablation (freezing of tissue at 20°C and 60°C). Most procedures are performed using a percutaneous approach. However, in some instances ablation with laparoscopy is recommended [4-6].

The RFA has been introduced for curing the primary hepatic cancer with diameter less than 3cm

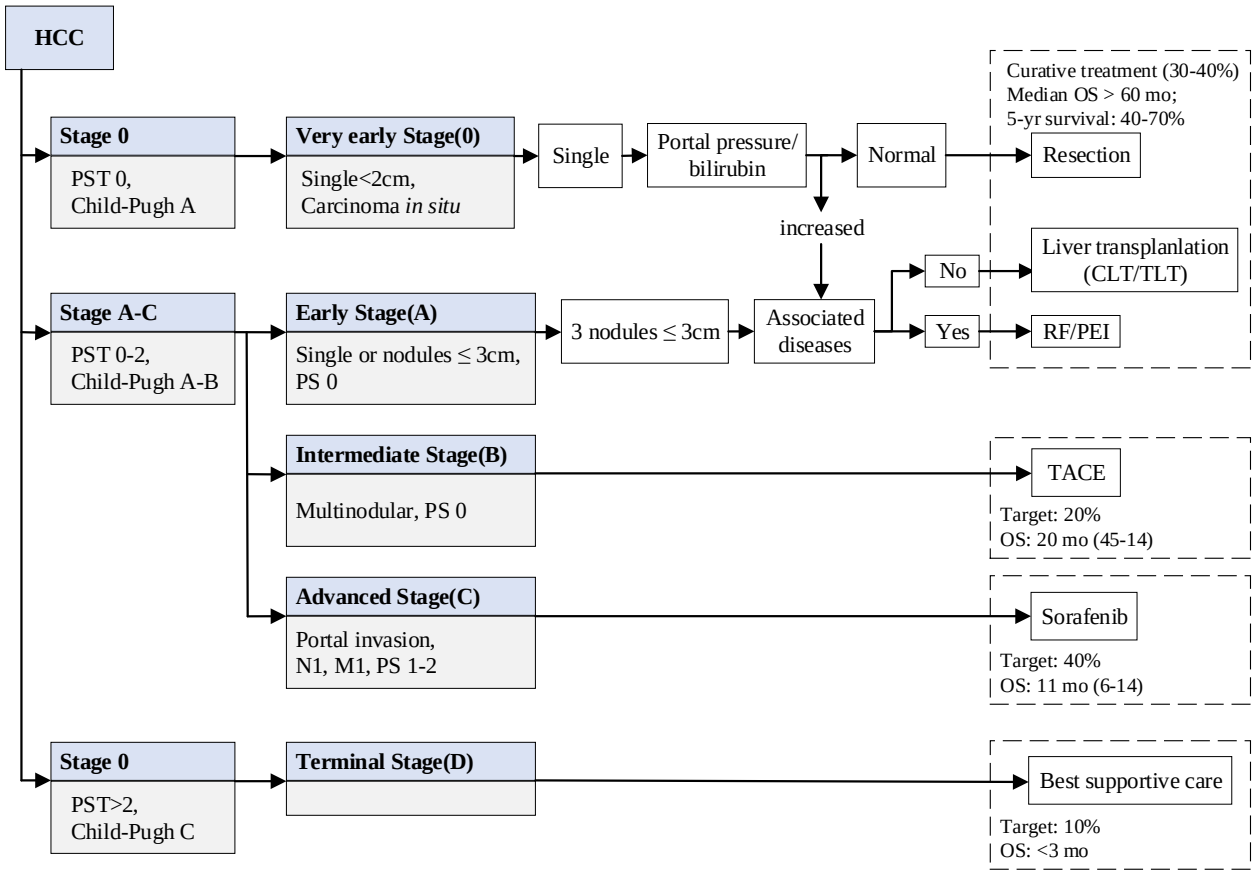

Figure. 1 The Barcelona clinic liver cancer staging system for HCC and treatment approach

[5–8]. In RFA, electric current at frequencies of 350 - 500 kHz is delivered into the cancer cells by an electrode placed inside the tumor, delivering the sufficient heat to kill the cancer cells [9-10]. Therefore, RFA is much less invasive than surgical resection. However, RFA technique incur the difficulty in treating large tumors and the potential for incomplete RF tumor ablation at near blood vessels due to the heat sink effection on the local blood flow [5, 11, 12].

As a result, MWA is alternative and is emerging as a new treatment option for patients with unrespectable hepatic malignancies [13-15]. In the treatment process, microwave (MW) is passed to the cancer tissues by an antenna, generating the heat to the target areas. MWA can active for a much larger zone of heating than RFA, due to the much broader field of power density of the electromagnetic field in MWA [5, 8]. In addition, properly designs of MW antenna can successfully manage the electromagnetic field distributions govern the temperature distributions for the unwanted tissue.

Many researches on MWA have been reported over the past decade. For example, according to [16] introduced three types of MW antennas, which are, open-tip monopole (OTM), dielectric-tip monopole (DTM), and metal-tip monopole (MTM), operating at 2.45 GHz for cardiac ablation. The finite element method (FEM)is used for analyzing different antenna characteristic. According to [17] proposed cap-choke catheter antenna the for MW treatment with localized heating of tissue surrounding the distal end of the catheter. Meanwhile, the floating sleeve antenna was proposed by [18], where the inclusion of the floating sleeve could prevent the flow of electromagnetic energy along the coaxial applicator. For asymmetry slot antenna, according to [19] investigated the characteristics of various slot size and various power for the antennas' temperature distributions and specific absorption rate (*SAR*). The study of heat transfer for liver tissue of asymmetry coaxial-slot antenna has been experimented by [20]. According to [21] introduced a new, minimally invasive coaxial antenna featuring a miniaturized choke of simple design. The proposed design attains minimum overall transversal size and allows small real time adjustments of the choke section length to compensate for little impedance mismatches which may arise during operation.

Many optimal MWA design methods have been proposed by several researchers. According to [22] proposed the antenna design with smallest possible insertion using impedance match between the feed line and antenna to allow the maximum power rating of a given feed to be used. Onward, according to [23] utilized this procedure to optimize the design of a minimally invasive choke antenna that can be used to create near-spherical ablation zones of adjustable size. The improvements of ablation using multiple MW antennas are also proposed in many researches. In [24] used the "MW coagulation therapy (MCT)" system, operating at 2.45 GHz with parallel slot antennas. Many researcher [7-8, 25] reported that using triple-antenna ablation in a triangular array in in vivo experiments produced synergistically larger ablation zones than those produced by single antenna ablation, thus indicating at the more convenient and effective treatment of large tumors using MWA [26]. The relation between the temperature distribution in the tissue and the distance of the electrodes and arteries are also conducted in many researches [8, 11, 12, 27, 28].

In RFA and MWA studies, numerical simulation has been widely used due to its fast and economical to evaluate new hypothetical designs. Simulations of 3-D coupled thermal–electric FEM analysis can be used for RFA [29-32]. However, all previous FEM analysis for MW hepatic ablation have been performed in two dimensions (approximating the geometry of the FEM model to be axisymmetric) [17, 18, 24]. The 3-D FEM has been used for more effective simulation of MWA [27, 28], afterward. Nevertheless, the simulation study on MWA requires intensively computation tool for handle of the FEM with many contradictory parameters. The better design results of some indicator may lead to the worst result in other indicators. The design with only expert experience and try and error correction may not be an effective process.

The earlier researches are still on the studies of slot size and position effect to the ablation zone concerning treatment temperature shape and volume. In [33] The effect slot positions and dimensions have on the size of the ablation zone, reflected power and highest temperature reached by microwave antennas in a hepatic tissue phantom is analyzed using commercial finite element model software. Two antenna configurations are analyzed, coaxial double slot and single slot with choke while taking into account antenna heating. The S_{11} analysis of multi-physics problem on microwave tissue heating with novel concept of multi-slot coaxial antenna with periodic slots had been presented, in [34]. The research in [35] present a coax-fed MWA antenna design for decreases the radiation of the monopole behind the reflector, creating an asymmetric *SAR* pattern by extending a portion of the outer conductor of the coaxial cable. In [36], the efficiency of different antennas for microwave ablation therapy were investigated using numerical simulation and

experimental approach. The evaluation is on the reflection coefficient, power dissipation distribution, power dissipation density, specific absorption rate, and temperature distribution in tissue. The later interesting researches on MW ablation is [37]. In [37], the aperiodic distributed tri-slot antenna was proposed. The method aimed at rounder ablation zones for MW ablation. The simulation was carried out by axisymmetric finite element model (FEM). However, the performance of MW ablation is multi-objective in nature and soft computation for decision making can take this advantage on OASPS.

More specifically, in the optimal antenna slot position and sizing (OASPS) design for hepatocellular carcinoma microwave ablation, the trading among temperature, volume and shape are required. Therefore, using multi-objective fuzzy decision making (MOFDM) can be the effective method for OASPS. In this paper, the multiple-objective optimal design of an asymmetry slot antenna is presented. The objective is to achieve a near-spherical zone for ablation, defined by axial ratio (*AR*), satisfying the minimum reflection coefficient (S_{11}), and maximum volume of destroying (*VD*). With the multi-objective optimization problem, the MOFDM is used for OASPS design. The FEM is used for simulation of MW distribution

2. Numerical assessment of antenna performance

In this section, we describe the computer model and optimization techniques used to design the optimal asymmetry slot antenna.

2.1 Bio-heat characteristic in tissue

The FEM [38] is used to analyze the bio-heat characteristic in the tissue. The heat generated in the tissue represented by the bio-heat equation as [39],

$$\rho C \frac{\partial T}{\partial t} + \nabla.(-k\nabla T) = -Q_p + Q_m + Q_{ext} \quad (1)$$

In this paper, cooling from liver tissue perfusion takes away a certain amount of heat from hepatic tissue, Q_p and Q_m are neglected in the finite element method calculation, due to their minimal value affecting the bio-heat characteristic comparing to other variables.

2.2 Specific absorption rate

The antenna heat distribution performance is represented by the specific absorption rate (*SAR*). The *SAR* represents the heat generated, in W/kg, by the electromagnetic field in the bio-tissue as [40],

$$SAR = \frac{\sigma.E^2}{\rho}, \quad (2)$$

In this paper, the *SAR*, generated in the bio-tissue due to the electromagnetic fields, has been investigated for antenna's wave analysis including heat and electricity characteristics. The *SAR* can be modeled in to the bio-heat equation as,

$$Q_{ext} = \rho SAR, \quad (3)$$

and

$$\rho C \frac{\partial T}{\partial t} + \nabla.(-k\nabla T) = \rho.SAR. \quad (4)$$

2.3 Axial ratio

Size and shape of the ablation zone, as well as the antenna's efficiency, are used to assess antenna performance [23]. Fig. 2 shows the size and shape relation of the ablation zone. The radius of the ablation zone or lesion radius (a) is defined as the maximal extent of the ablation zone in the radial direction. The Axial Ratio *AR*, representing the sphericity of the ablation zone, is defined as the ratio of the radius of the ablation zone to the width of the ablation zone (b). The *AR* is given by *AR = a/b*. The width of the ablation zone is measured 1mm away from the antenna surface to mitigate the impact of slight tails in the thermal profile. Axial ratio of 0.5 corresponds to an absolute half sphere. Note that this measure of sphericity takes into account only the radial and axial extents of the ablation zone, and thus, slight deviations in shape of the ablation zone away from these regions are not reflected in this metric. In this paper, the 50°C isotherm is used to represent the boundary of the ablation zone. The target is to obtain the destroy shape as close to spear as possible. The near spare index (*ARC*) can be given by,

$$ARC = |AR - 0.5|, \quad (5)$$

2.4 Reflection coefficient

Reflection Coefficient S_{11}, also called S-parameters, is one of the parameters used in two-port network [41]. The S_{11} relates to the traveling waves

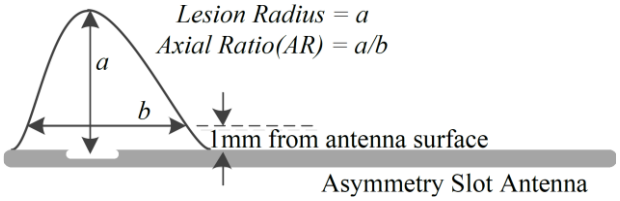

Figure. 2 size and shape of ablation zone

Received: March 2, 2020. Revised: April 21, 2020.

that are scattered or reflected when a network is inserted into a transmission line of certain characteristic impedance (Z_L). Therefore, S_{11} can be compared to reflection and through pass of a pair of spectacles.

The efficiency of an antenna can be obtained the ratio of power reflected to power input, S_{11} is important in microwave design because they are easier to measure and to work with at high frequencies than other kinds of two-port parameters. It is conceptually simple, analytically convenient and capable of providing detailed insight into a measurement and modeling problem, typically measured on a "decibel scale" as,

$$S_{11} = 10\log\left(\frac{P_r}{P_i}\right). \quad (6)$$

Since S_{11} is measured on a decibel scale, smaller S_{11} indicates greater power coupled to the tissue. Reflected power was calculated from the FEM model by sampling the net time-averaged power flow at the antenna feed point and subtracting from the input power. The net-time averaged power flow, which is proportional to the square of the electric field, is determined by integrating the net power over each node at the source boundary.

2.5 Volume of destroying (*VD*)

In this paper, the *VD* at 50°C is introduced to evaluate the performance of antenna .The *VD* can be determined by integration of the isotherm surface obtained from finite element model.

3. MOFDM formulation for OASPS

Due to multiple contradictory parameters behavior in antenna design, realistic antenna design solutions require special attention to the multi-objective optimization. From a practical point of view, an antenna design does not need to find a rigid single objective optimization solution. Certain trade-off among objective function and constraints would be desirable. Therefore, the multi-objective fuzzy decision making [42] is used to determine the optimal slot and size of the antenna. The proposed MOFDM for OASPS problem formulation can be expressed as,

The objective functions are,

(1) to achieve the circular condition of MW as,
Minimize *ARC* in Eq.(5),

(2) to achieve the high power coupled to the tissue as,
Minimize S_{11} in Eq. (6), and

(3) to obtain the large *VD* as,
Maximize *VD,* as described in Section 2.5.

In the proposed MOFDM based OASPS, the objective functions in Eqs. (6) - (8) are fuzzified in to the degree of satisfactions or fuzzy membership functions as shown in Figs. 3 - 5. In Fig. 3, the closer *AR* to 0.5, the closer to circular shape, therefore, the higher degree of satisfaction. Meanwhile, in Fig. 4, the lower S_{11} lead to the higher degree of satisfaction. In contrast, the larger *VD* is the higher satisfaction, as shown in Fig. 5.

As a results, the objective functions in Eqs.(6) - (8) can be represented by fuzzy maximization problem as,

$$\text{Maximize } \mu = \min\{\mu_{AR}, \mu_{VD}, \mu_{S_{11}}\}. \quad (9)$$

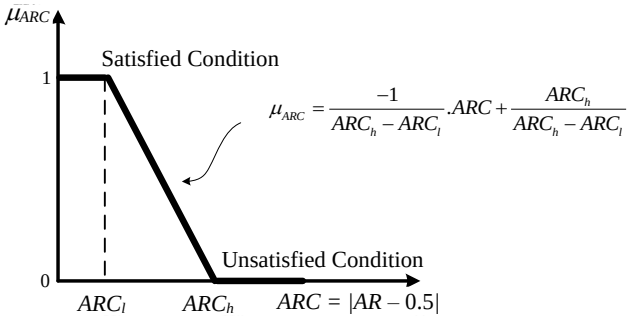

Figure. 3 Fuzzy membership function representing degree of satisfaction of *ARC*

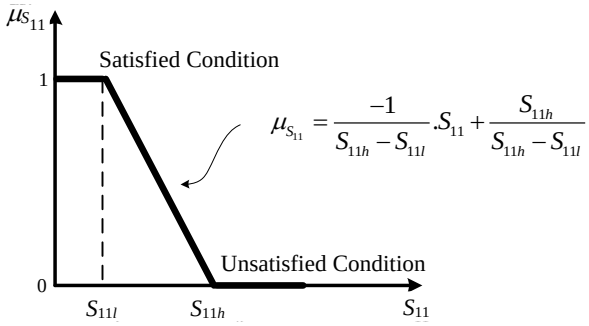

Figure. 4 Fuzzy membership function representing degree of satisfaction of S_{11}

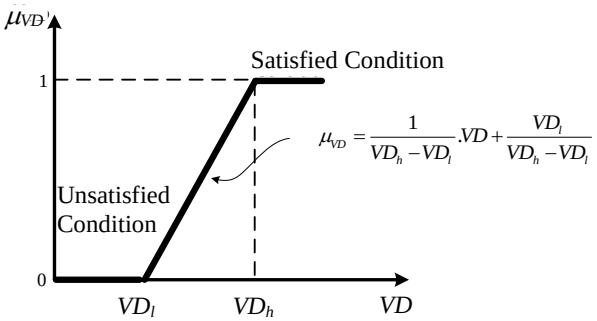

Figure. 5 Fuzzy membership function representing degree of satisfaction of *VD*

Where,

$$\mu_{ARC}=\begin{cases}1 & ,\ for\ ARC\le ARC_l\\ \dfrac{-1}{ARC_h-ARC_l}.ARC & \\ \quad+\dfrac{ARC_h}{ARC_h-ARC_l} & ,\ for\ ARC_l\le ARC<ARC_h\\ 0 & ,\ for\ ARC\ge ARC_h\end{cases}, \tag{10}$$

$$\mu_{S_{11}}=\begin{cases}1 & ,\ for\ S_{11}\le S_{11l}\\ \dfrac{-1}{S_{11h}-S_{11l}}.S_{11} & \\ \quad+\dfrac{S_{11h}}{S_{11h}-S_{11l}} & ,\ for\ S_{11l}\le S_{11}<S_{11h}\\ 0 & ,\ for\ S_{11}\ge S_{11h}\end{cases}, \tag{11}$$

$$\mu_{VD}=\begin{cases}0 & ,\ for\ VD\le VD_l\\ \dfrac{1}{VD_h-VD_l}.VD & \\ \quad+\dfrac{VD_l}{VD_h-VD_l} & ,\ for\ VD_l\le VD<VD_h\\ 1 & ,\ for\ VD\ge VD_h\end{cases}, \tag{12}$$

The ARC_h, S_{11h}, and VD_h are given by the maximum values of ARC, S_{11}, and VD obtained from the simulation, respectively. Similarly, ARC_l, S_{11l}, and VD_l are given by the minimum values of ARC, S_{11}, and VD obtained from the simulation, respectively.

4. Simulation results on MOFDM for OASPS

The MOFDM for OASPS is tested on designing of the antenna build up from the coaxial cable. The coaxial cable used is Semi-rigid 141) RG402 M17/130-RG402 Copper Jacket) including Inner conductor, Dielectric, and Outer conductor, as shown in Fig. 6.

The cable is short circuit at the end and revealed half of the outer conductor by 180°. The slot distance from conductor end is L_{ts}. Slot size is defined by the width of open surface (W_d). The antenna's parameters and dimension are shown in Table 1.

The Comsol® programs are used to calculate the heat distribution and electromagnetic field absorption ratio of lever tissue including RF Module and Heat Transfer using Bio-heat Equation). The processor used is Intel® Core(TM)i5-3210M CPU @ 2.50 GHz with RAM 8 GB. The parameters used in the computation are shown in Table 2. The results obtained from 3D FEM are shown in Table 3.

To determine an appropriate slot position and size, the destroy shape should be as close as to the absolute half sphere, which can be represented by the AR. In addition, the S_{11} representing the wave reflectance, or return loss, of the antenna should be at minimum.

In the simulation, L_{ts}, representing the slot position, is varied as 2.3mm, 3.3mm, 4.3mm,5.3 mm, 6.3mm, 7.3mm, and 8.3mm. Meanwhile, W_d, representing the slot size, is varied as 1mm, 2mm, 3mm, 4mm, 5mm, and 6mm. The input power (P_i) used is 50 W with the duration of 300 seconds. The comparison of AR obtained by different L_{ts} and W_d, is illustrated in Fig. 7.

In Table 3, the slot position at 2.3mm with slot size of 5mm and 6mm cannot be computed due to the positions are beyond the antenna length. It is observed that the AR is the lowest of 0.487 at the L_{ts} of 8.3mm with W_d of 6mm. Meanwhile, AR is the highest of 0.792 at the L_{ts} of 8.3mm with W_d of 1mm VD is shown to be lowest of 91.669mm^3 at L_{ts} and W_d of 8.3mm and 1mm, respectively. In contrast, VD is the highest of 1166.677mm^3 at L_{ts} is 3.3mm and W_d is 6mm. The S_{11} is the lowest of -0.163 at L_{ts} of 8.3mm with W_d of 1mm, and the highest of -0.675 at L_{ts} of 3.3mm with W_d of 6mm. It is obviously that the

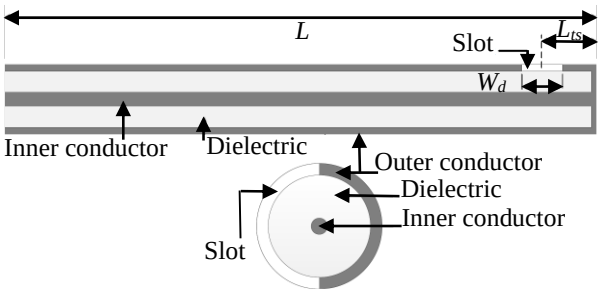

Figure. 6 Asymmetry slot antenna

Table 1. The antenna's parameters and dimension

Diameter inner conductor (Silver) Plated	0.912mm
Diameter of dielectric (Solid PTFE)	2.985mm
Diameter of outer conductor	3.581mm
Length from the tip to the center of the	5.3mm
Length of antenna (L)	70mm
Width of the slot (W_d)	3mm

Table 2. The parameters used in the computation

ρ	1050	kg/m^3
C	3700	J/kg.K
k	0.56	W/m.K
ρ_b	1000	Kg/m^3
C_b	3639	J/kg.K
ω_b	0.0036	m^3/kg.S
σ_{liver}	1.69	S/m
ε_{liver}	43.03	
$\varepsilon_{dielectric}$	2.03	
$\varepsilon_{insulator}$	2.60	

Received: March 2, 2020. Revised: April 21, 2020.

Table 3. The *AR*, S_{11}, and *VD* results obtained from FEM

L_{ts} (mm)	W_d (mm) 1			2			3		
	AR	S_{11}	*VD*(mm^3)	*AR*	S_{11}	*VD*(mm^3)	*AR*	S_{11}	*VD*(mm^3)
2.3	0.690	-0.213	189.242	0.601	-0.357	496.570	0.545	-0.437	672.619
3.3	0.699	-0.193	145.401	0.592	-0.340	436.273	0.546	-0.447	665.745
4.3	0.692	-0.199	150.871	0.594	-0.309	356.783	0.555	-0.379	503.077
5.3	0.729	-0.188	131.068	0.607	-0.291	316.491	0.558	-0.379	487.368
6.3	0.759	-0.177	114.306	0.626	-0.268	274.299	0.564	-0.350	424.446
7.3	0.772	-0.170	103.451	0.631	-0.256	254.259	0.577	-0.306	351.088
8.3	0.792	-0.163	91.669	0.631	-0.242	231.445	0.566	-0.315	367.049
L_{ts} (mm)	W_d (mm) 4			5			6		
	AR	S_{11}	*VD*(mm^3)	*AR*	S_{11}	*VD*(mm^3)	*AR*	S_{11}	*VD*(mm^3)
2.3	0.515	-0.553	925.938	-	-	-	-	-	-
3.3	0.525	-0.497	773.498	0.514	-0.611	1020.615	0.496	-0.675	1166.676
4.3	0.523	-0.492	734.938	0.512	-0.523	805.118	0.494	-0.577	921.179
5.3	0.541	-0.453	637.490	0.521	-0.346	357.420	0.501	-0.416	497.699
6.3	0.532	-0.421	568.495	0.510	-0.469	658.652	0.499	-0.509	743.854
7.3	0.526	-0.393	512.558	0.501	-0.442	604.369	0.493	-0.484	681.898
8.3	0.528	-0.377	481.079	0.501	-0.420	565.006	0.487	-0.459	603.155

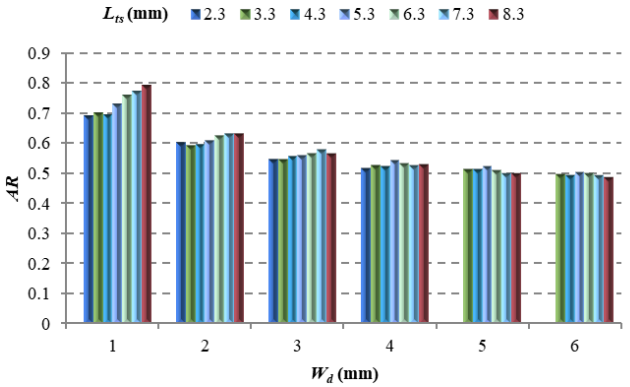

Figure. 7 The *AR* of different slot size and position

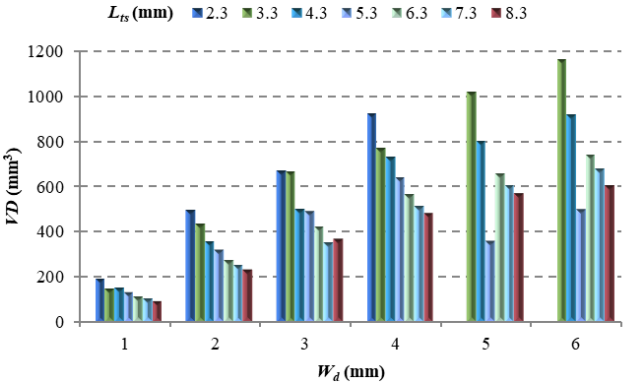

Figure. 9 The *VD* of different slot size and position

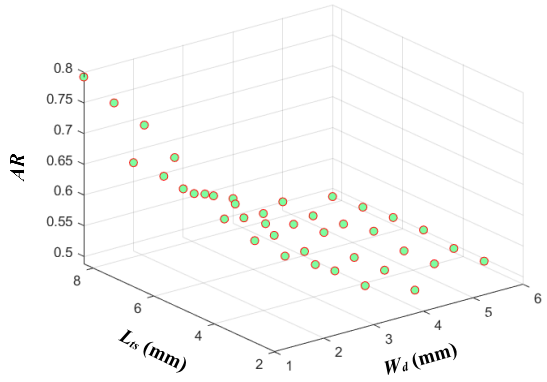

Figure. 8 The relation of *AR* with different L_{ts} and W_d

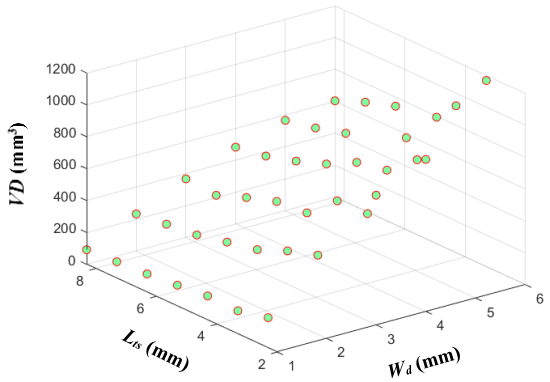

Figure. 10 The relation of *VD* with different L_{ts} and W_d

objectives are contradictory in nature. Table 4 addresses the *VD* and shape of different L_{ts} and W_d in graphical illustration.

Fig. 8 illustrates the relation of *AR* with different L_{ts} and W_d. *AR* is 0.501, closest to 0.5 at two conditions, which are, at L_{ts} = 5mm and W_d = 6mm, and at L_{ts} = 7.3mm and W_d = 5mm.

Fig. 9 presents the *VD* at 50 °C of different L_{ts} and W_d. the results show that the *VD* is comparatively high to other, with the L_{ts} of 2.3mm and 3.3mm. The results also show that *VD* is the highest of 1166.675mm^3 at L_{ts} = 3.3mm and W_d = 6mm. Fig. 10. illustrates the relation of *VD* with different L_{ts} and W_d. Meanwhile, Fig. 11. shows the slot size (S_{11}) of different slot size and position. The S_{11} is shown to be

 DOI: 10.22266/ijies2020.1031.05

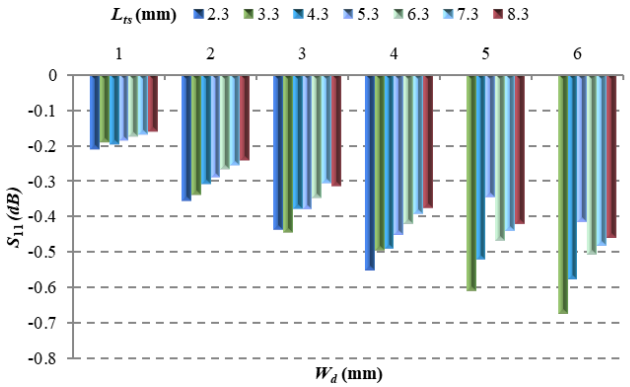

Figure. 11 The S_{11} of different slot size and position

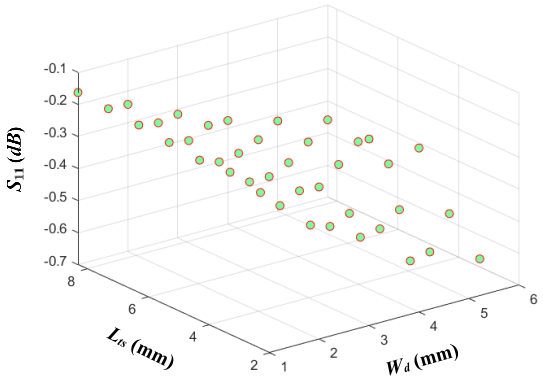

Figure. 12 The relation of S_{11} with different L_{ts} and W_d

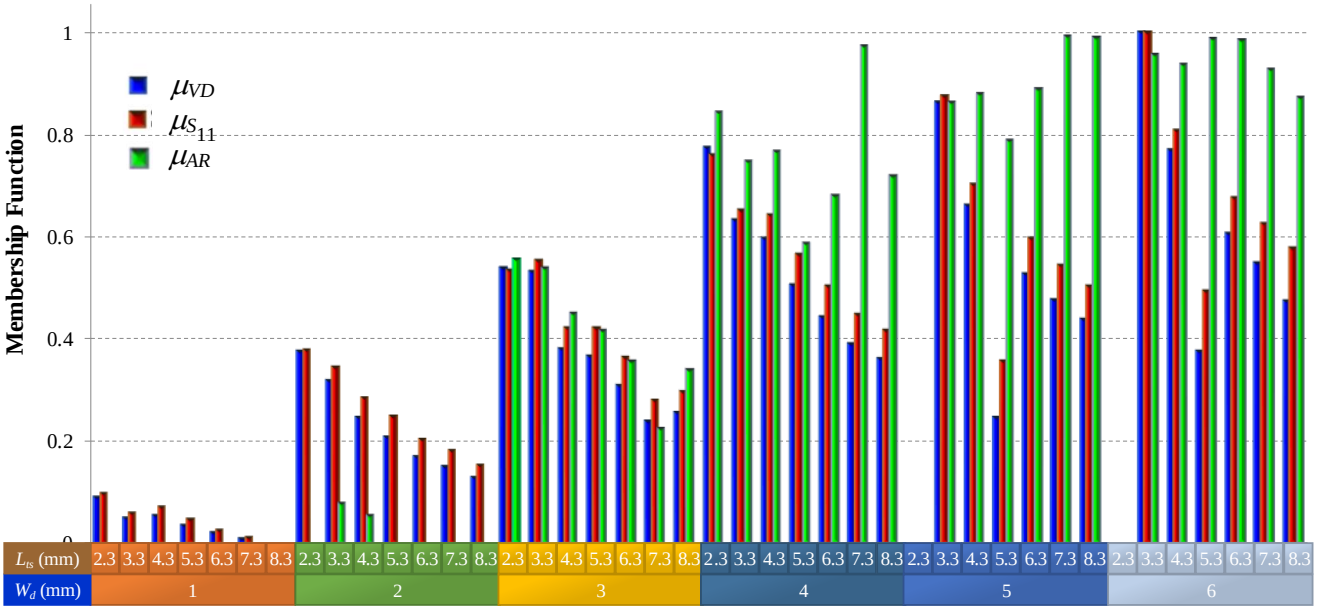

Figure. 13 μ_{AR}, μ_{VD}, and $\mu_{S_{11}}$, of different design

Table 4. μ_{AR}, μ_{VD}, and $\mu_{S_{11}}$ for different L_{ts} and W_d

L_{ts} (mm)	W_d (mm) 1			2			3		
	μ_{AR}	$\mu_{S_{11}}$	μ_{VD}	μ_{AR}	$\mu_{S_{11}}$	μ_{VD}	μ_{AR}	$\mu_{S_{11}}$	μ_{VD}
2.3	0.000	0.098	0.091	0.000	0.379	0.377	0.555	0.536	0.540
3.3	0.000	0.060	0.050	0.000	0.346	0.321	0.540	0.555	0.534
4.3	0.000	0.071	0.055	0.056	0.286	0.247	0.452	0.423	0.383
5.3	0.000	0.049	0.032	0.000	0.250	0.209	0.417	0.422	0.368
6.3	0.000	0.028	0.021	0.000	0.205	0.170	0.359	0.365	0.310
7.3	0.000	0.014	0.011	0.000	0.182	0.151	0.227	0.280	0.241
8.3	0.000	0.000	0.000	0.000	0.155	0.130	0.341	0.297	0.256
L_{ts} (mm)	W_d (mm) 4			5			6		
	μ_{AR}	$\mu_{S_{11}}$	μ_{VD}	μ_{AR}	$\mu_{S_{11}}$	μ_{VD}	μ_{AR}	$\mu_{S_{11}}$	μ_{VD}
2.3	0.846	0.762	0.776	-	-	-	-	-	-
3.3	0.749	0.652	0.634	0.865	0.875	0.864	0.958	1.000	1.000
4.3	0.769	0.643	0.598	0.882	0.703	0.664	0.938	0.810	0.772
5.3	0.589	0.567	0.508	0.789	0.357	0.247	0.988	0.495	0.378
6.3	0.683	0.504	0.444	0.890	0.598	0.527	0.987	0.677	0.607
7.3	0.974	0.450	0.392	0.993	0.546	0.477	0.929	0.627	0.549
8.3	0.720	0.418	0.362	0.992	0.503	0.440	0.874	0.579	0.476

the minimum of -0.675 when L_{ts} = 3.3mm and W_d =6mm. The relation of S_{11} with different L_{ts} and W_d is

illustrated in Fig. 12.

With the contradictory objectives of *AR*, S_{11}, and *VD*, the FDM is applied to obtain the multi-objective optimal design of antenna slot position and sizing. The value of *AR*, S_{11}, and *VD* are, then, fuzzified in to the membership functions or degree of satisfaction described in Section III. The membership function of *AR*, *VD*, and S_{11} are represented by μ_{AR}, μ_{VD}, and $\mu_{S_{11}}$, respectively. The maximin method is used to trade-off among the objectives.

Table 4 addresses the μ_{AR}, μ_{VD}, and $\mu_{S_{11}}$, for different L_{ts} and W_d. Fig. 13. Illustrates the comparison on μ_{AR}, μ_{VD}, and $\mu_{S_{11}}$, of different design.

With the maximin theorem, the optimal design of antenna is at L_{ts} of 3.3mm and W_d of 6mm. The optimal output results in the overall membership function of 0.958, indicating the maximum degree of satisfaction among minimum degree of satisfactory.

The proposed MOFDM for OASPS design output is compared to the design proposed in [20], due to the method proposed in [20] provide the comparison of open slot angle for asymmetry slot antenna using 3D finite element method with the close angle of 90, 180, 270, and 360 degrees, as shown in Figs. 14-17. However, the proposed method is, in fact, can be applied to other design purposes for OASPS. The design result of [20] is L_{ts} = 5.3mm and W_d = 3mm. Meanwhile, the result recommended by the proposed MOFDM for OASPS is L_{ts} = 3.3mm and W_d = 6mm. In Fig. 14., it is observed that the temperature distribution of the proposed MOFDM for OASPS is in the more controllable shape than [20], due to the sharp beam of temperature distribution to the target at the front side of slot with the less temperature distribution at the rare side of slot. The *SAR* results in Fig. 15 also shows that the proposed MOFDM for OASPS design is easier to manage with the less effect to the rare side of the slot. Fig. 16 shows the graphical simulation results of the temperature distributions of the design results from [20] and the proposed MOFDM for OASPS. It is observed that the proposed MOFDM for OASPS resulted in the temperature distribution shape closer to round shape than that of the result from [20].

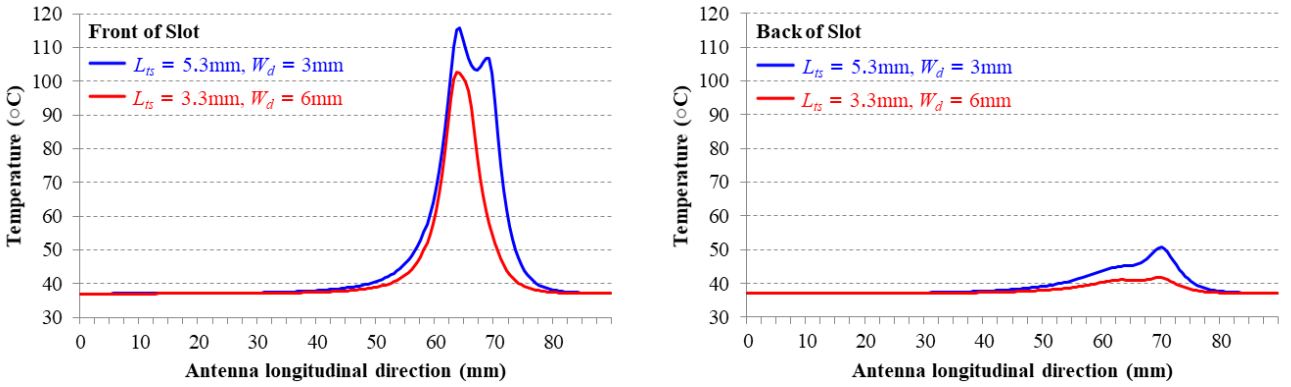

Figure. 14 Comparison on Temperature distributions of [20] (L_{ts} = 5.3mm and W_d = 3mm) and the proposed MOFDM for OASPS (L_{ts} = 3.3mm and W_d = 6mm)

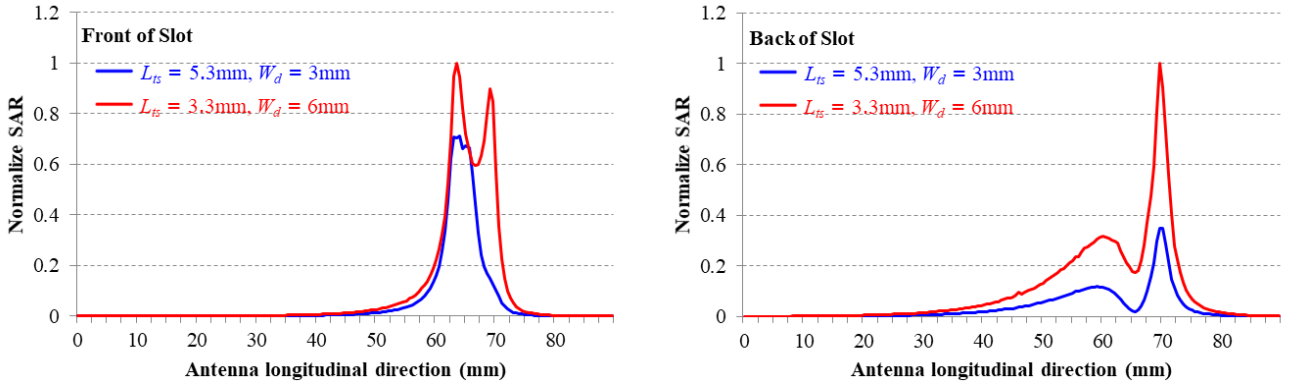

Figure 15 Comparison on *SAR* of [20] (L_{ts} = 5.3mm and W_d = 3mm) and the proposed MOFDM for OASPS (L_{ts} = 3.3mm and W_d = 6mm)

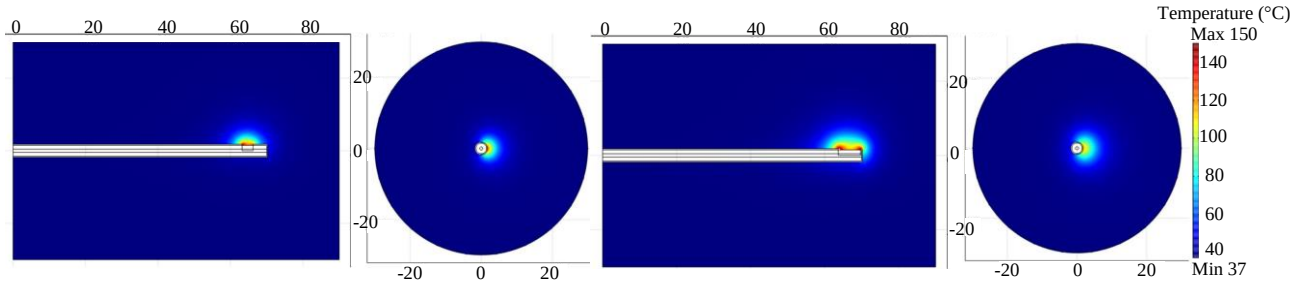

(a) (b)

Figure. 16 Simulation results of: (a) temperature distribution shapes of [20] (L_{ts} = 5.3mm and W_d = 3mm) and (b) the proposed MOFDM for OASPS (L_{ts} = 3.3mm and W_d = 6mm) Note: length in mm

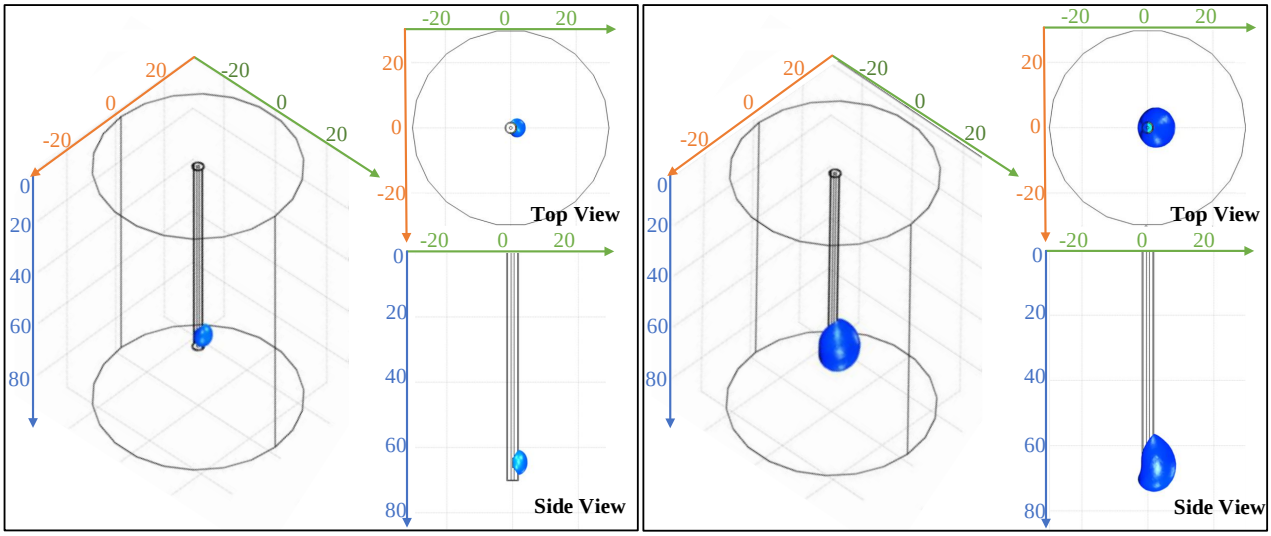

(a) (b)

Figure. 17 Simulation results of temperature distribution by: (a) finite element model of [20] (L_{ts} = 5.3mm and W_d = 3mm) and (b) the proposed MOFDM for OASPS (L_{ts} = 3.3mm and W_d = 6 mm) Note: length in mm

5. Conclusion

In this paper, the non-conventional slot design using fuzzy decision making for multi-objective functions include, minimization the circular condition of MW, minimization of the high power coupled to the tissue, and maximization of the volume of destroy, is proposed. The circular condition of MW with satisfied power and volume of cancer cell destroying can be achieved, simultaneously. The experimentation was carried out by software simulation using Comsol® programs incorporating multi-objective fuzzy decision making algorithm, with several antenna slot position and size data collection. Therefore, the circular condition of MW with satisfied power and volume of cancer cell destroying can be achieved, simultaneously. The simulation results show that the proposed MOFDM can provide the near-spherical zone of ablation trading-off with the minimum S_{11}, and maximum VD in MW antenna design. The temperature distribution shape resulted by the proposed MOFDM for OASPS is closer to the spear and better utilization with the front side of slot sharp beam than that of existing design. Therefore, the proposed method can efficiency be used for fast preliminary antenna slot design for hepatocellular carcinoma microwave ablation before detail analysis and the computation time for MW antenna slot size and position can be substantially reduced. The proposed method can be further extended to the different proposed of slot designs.

Conflicts of Interest

The authors declare no conflict of interest.

Author Contributions

Conceptualization, Petch Nantivatana, Pattarapong Phasukkit, Supan Tungjitkusolmun,and Keerati Chayakulkheeree; methodology, Petch Nantivatana and Keerati Chayakulkheeree; software, Petch Nantivatana and Pattarapong Phasukkit; validation, Petch Nantivatana, Supan Tungjitkusolmun, and Keerati Chayakulkheeree; formal analysis, Petch Nantivatana, Pattarapong

Phasukkit, Supan Tungjitkusolmun,and Keerati Chayakulkheeree; investigation, Petch Nantivatana; resources, Petch Nantivatana; data curation, Petch Nantivatana; writing—original draft preparation, Petch Nantivatana; writing—review and editing, Petch Nantivatana and Keerati Chayakulkheeree; visualization, Petch Nantivatana; supervision, Supan Tungjitkusolmun; project administration, Petch Nantivatana.

References

[1] M. F. Yuen, J. L. Hou, and A. Chutaputti, "Hepatocellular carcinoma in the Asia pacific region", *Journal of Gastroenterology and Hepatology*, Vol.24, Issue 3, pp. 346-353, 2009.

[2] R. M. Abreu, C. S. Ferreira, P. D. Nasser, L. O. O. Kikuchi, F. J. Carrilho, and S. K. Ono, "Hepatocellular Carcinoma: The Final Moments of Life", *Journal of Cancer Therapy*, Vol. 4, pp. 377-383, 2013.

[3] European Association for the Study of the Liver, "European Organization for Research and Treatment of Cancer: EASL–EORTC Clinical Practice Guidelines: Management of hepatocellular carcinoma", *Journal of Hepatology*, Vol. 56, pp. 908–943, 2012.

[4] G. Ma and G. Jiangl, "Review of Tumor Hyperthermia Technique in Biomedical Engineering Frontier", In: *Proc. of 2010 3rd International Conference on Biomedical Engineering and Informatics (BMEI 2010)*, Yantai, China, pp. 1357-1359, 2010.

[5] T. J. Vogl, T. K. Helmberger, M. G. Mack, and M. F. Reiser Eds, "Ablative techniques (percutaneous) thermal ablative techniques", *Percutaneous Tumor Ablation in Medical Radiology*, pp. 7–32, 2008.

[6] D. M. Mahvi and F. T. Lee, Jr., "Radiofrequency ablation of hepatic malignancies: Is heat better than cold?", *Ann. Surg.*, Vol. 230, No. 1, pp. 9–11, 1999.

[7] A. S. Wright, D. M. Mahvi, D. G. Haemmerich, and F. T. Lee, Jr., "Minimally invasive approaches in management of hepatic tumors", *Surg. Technol. Int.*, Vol. 11, pp. 144–153, 2003.

[8] D. Haemmerich and F. T. Lee, Jr., "Multiple applicator approaches for radiofrequency and microwave ablation", *Int. J. Hyperthermia*, Vol. 21, No. 2, pp. 93–106, 2005.

[9] M. W. Miller and M. C. Ziskin, "Biological consequences of hyperthermia", *Ultrasound Med. Biol.*, Vol. 15, pp. 707–722, 1989.

[10] S. A. Sapareto and W. C. Dewey, "Thermal dose determination in cancer therapy", *Int. J. Radiat. Oncol. Biol. Phys.*, Vol. 10, pp. 787–800, 1984.

[11] C. Cha, F. T. Lee, Jr., L. F. Rikkers, J. E. Niederhuber, B. T. Nguyen, and D. M. Mahvi, "Rationale for the combination of cryoablation with surgical resection of hepatic tumors", *J. Gastrointest. Surg.*, Vol. 5, No. 2, pp. 206–213, 2001.

[12] S. B. Chinn, F. T. Lee, Jr., G. D. Kennedy, C. Chinn, C. D. Johnson, T. C. Winter, III, T. F. Warner, and D. M. Mahvi, "Effect of vascular occlusion on radiofrequency ablation of the liver: Results in a porcine model", *AJR Amer. J. Roentgenol*, Vol. 176, pp. 789–795, 2001.

[13] P. Prakash, "Theoretical Modeling for Hepatic Microwave Ablation", *The Open Biomedical Engineering Journal*, Vol. 4, pp. 27-38, 2010.

[14] A. S. Wright, L. A. Sampson, T. F. Warner, D. M. Mahvi, and F. T. Lee, Jr., "Radiofrequency versus microwave ablation in a hepatic porcine model", *Radiology*, Vol. 236, pp. 132–139, 2005.

[15] M. Lu, J. Chen, X. Xie, L. Liu, X. Huang, L. Liang, and J. Huang, "Hepatocellular carcinoma: US-guided percutaneous microwave coagulation therapy", *Radiology*, Vol. 221, No. 1, pp. 167–172, 2001.

[16] S. Labont´e, A. Blais, S. R. Legault, H. O. Ali, and L. Roy, "Monopole antennas for microwave catheter ablation", *IEEE Trans. Microw. Theory Tech.*, Vol. 44, No. 10, pp. 1832–1840, 1996.

[17] J. C. Lin, and Y.-J. Wang, "The cap-choke catheter antenna for microwave ablation treatment", *IEEE Trans. Biomed. Eng.*, Vol. 43, No. 6, pp. 657–660, 1996.

[18] D. Yang, J. M. Bertram, M. C. Converse, A. P. O'Rourke, J. G. Webster, S. C. Hagness, J. A. Will, and D. M. Mahvi, "A floating sleeve antenna yields localized hepatic microwave ablation", *IEEE Trans. Biomed. Eng.*, Vol. 53, No. 3, pp. 533–537, 2006.

[19] P. Nantivatana, S. Tungjitkusolmun, P. Phasukkit, and M. Sangworasil, "3D Finite Element Analysis for non-Asymmetry Structure Antenna for Microwave Ablation Therapy", In: *Proc. of the third International Symposium on Biomedical Engineering (ISBME 2008),* pp. 11-22, 2008.

[20] K. Thaiwat, P. Nantivatana, P. Phasukkit, S. Tungjitkusolmun, and M. Sangworasil, "Comparision of Open Slot Angle for Asymmetry Slot Antenna using 3D Finite Element Method", In: *Proc. of the 2011 Biomedical Engineering International Conference (BMEiCON2011),* pp. 100 – 103, 2012.

[21] I. Longo, G. B. Gentili, M. Cerretelli, and N.

Tosoratti, "A Coaxial Antenna with Miniaturized Choke for Minimally Invasive Interstitial Heating", *IEEE Trans. Biomed. Eng.*, Vol. 50, No. 1, pp. 82-88, 2003.

[22] C. L. Brace, P. F. Laeseke, D. W. van der Weide, and F. T. Lee, Jr., "Microwave Ablation With a Triaxial Antenna Results in ex vivo Bovine Liver", *IEEE Trans. Microw. Theory Tech.*, Vol. 53, No. 1, pp. 215-220, 2005.

[23] P. Prakash, M. C. Converse, J. G. Webster, and D. M. Mahvi, "An Optimal Sliding Choke Antenna for Hepatic Microwave Ablation", *IEEE Trans. Biomed. Eng.*, Vol. 56, No. 10, pp. 2470-2476, 2009.

[24] K. Saito, Y. Hayashi, H. Yoshimura, and K. Ito, "Heating characteristics of array applicator composed of two coaxial-slot antennas for microwave coagulation therapy", *IEEE Trans. Microw. Theory Tech.*, Vol. 48, No. 11, pp. 1800–1806, 2000.

[25] P. Phasukkit, S. Tungjitkusolmun, and M. Sangworasil, "Finite-Element Analysis and *In Vitro* Experiments of Placement Configurations Using Triple Antennas in Microwave Hepatic Ablation", *IEEE Trans. Biomed. Eng.*, Vol. 56, No. 11, pp. 2564-2572, 2009.

[26] A. S. Wright, F. T. Lee, Jr., and D. M. Mahvi, "Hepatic microwave ablation with multiple antennae results in synergistically larger zones of coagulation necrosis", *Ann. Surg. Oncol.*, Vol. 10, No. 3, pp. 275–283, 2003.

[27] P. Yhamyindee, P. Phasukkit, S. Tungjitkusolmon, and A. Sanpanich, "Analysis of Heat Sink Effect in Hepatic Cancer Treatment Near Arterial for Microwave Ablation by using Finite Element Method", In: *Proc. of the 2012 Biomedical Engineering International Conference (BMEiCON2012)*, 2012.

[28] J. Chiang, K. Hynes, and C. L. Brace, "Flow-Dependent Vascular Heat Transfer during Microwave Thermal Ablation", In: *Proc. of 34th Annual International Conference of the IEEE EMBS*, pp. 5582-5585, 2012.

[29] D. Panescu, J. G. Whayne, S.D. Fleischman, M. S. Mirotznik, D. K. Swanson, and J. G. Webster, "Three-dimensional finite element analysis of current density and temperature distributions during radio-frequency ablation", *IEEE Trans. Biomed. Eng.*, Vol. 42, No. 9, pp. 879–890, 1995.

[30] S. Tungjitkusolmun, E. J. Woo, H. Cao, J. Z. Tsai, V. R. Vorperian, and J. G. Webster, "Finite element analyses of uniform current density electrodes for radio-frequency cardiac ablation", *IEEE Trans. Biomed. Eng.*, Vol. 47, No. 1, pp. 32–40, 2000.

[31] E. J. Woo, S. Tungjitkusolmun, H. Cao, J. Z. Tsai, J. G. Webster, V. R. Vorperian, and J. A. Will, "A new catheter design using needle electrode for subendocardial RF ablation of ventricular muscles: Finite element analysis and *in vitro* experiments", *IEEE Trans. Biomed. Eng.*, Vol. 47, No. 1, pp. 23–31, 2000.

[32] D. Haemmerich, S. Tungjitkusolmun, S. T. Staelin, F. T. Lee, Jr., D. M. Mahvi, and J. G. Webster, "Finite-element analysis of hepatic multiple probe radio-frequency ablation", *IEEE Trans. Biomed. Eng.*, Vol. 49, No. 7, pp. 836–842, 2002.

[33] V. Neagu, "A Study of Microwave Ablation Antenna Optimization", In: *Proc. of the 6th IEEE International Conference on E-Health and Bioengineering - EHB 2017*, pp. 41-44, 2017.

[34] P. Gas, "Optimization of multi-slot coaxial antennas for microwave thermotherapy based on the S11-parameter analysis", *Biocybernetics and biomedical engineering,* Vol. 37, pp. 78-93, 2017.

[35] Y. Mohtashami, S. C. Hagness, and N. Behdad, "A Hybrid Slot/Monopole Antenna with Directional Heating Patterns for Microwave Ablation", *IEEE Transaction on Antenas and Propagation*, Vol. 65, No. 8, pp. 3889-3896, 2017.

[36] A.Z. Ibitoye, T. Orotoye, E.O. Nwoye, and M.A. Aweda, "Analysis of efficiency of different antennas for microwave ablation using simulation and experimental methods", *Egyptian Journal of Basic and Applied Sciences*, Vol. 5, pp. 24-30, 2018.

[37] Y. Xua, M. A.J. Moserb, E. Zhangc, W. Zhanga, and B. Zhangd, "Large and round ablation zones with microwave ablation: A preliminary study of an optimal aperiodic tri-slot coaxial antenna with the π-matching network section", *International Journal of Thermal Sciences*, Vol. 140, pp. 539–548, 2019.

[38] J.M. Jin, *The Finite Element Method in Electromagnetics*, 2nd edition, Wiley-IEEE Press, 2002.

[39] H. H. Pennes, "Analysis of tissue and arterial blood temperatures in the resting human forearm", *J. Appl. Phys.*, Vol. 1, pp. 93–122, 1948.

[40] P. R. Stauffer, F. Rossetto, M. Prakash, D. G. Neuman, and T. Lee, "Phantom and animal tissues for modelling the electrical properties of human liver", *Int. J. Hyperthermia*, Vol. 19, pp. 89-101, 2003.

[41] D. M. Pozar, *Microwave engineering*, 4th edition, John Wiley & Sons, Inc., 2011.

Received: March 2, 2020. Revised: April 21, 2020.

[42] H. J. Zimmermann, *Fuzzy Set Theory and its Applications,* 4th edition, Springer, 2001.